Physical properties of lanthanum monosulfide thin films grown on (100) silicon substrates

Cahay, M.; Garre, K.; Wu, X.; Poitras, Daniel; Lockwood, David; Fairchild, S.

Publisher's version / Version de l'éditeur:
https://doi.org/10.1063/1.2201998
Journal of Applied Physics, 99, 12, 2006

Physical properties of lanthanum monosulfide thin films grown on (100) silicon substrates

M. Cahay[a] and K. Garre
ECECS Department, University of Cincinnati, Cincinnati, Ohio 45221

X. Wu, D. Poitras, and D. J. Lockwood
Institute for Microstructural Sciences, National Research Council, Ottawa, Ontario K1A OR6, Canada

S. Fairchild
Air Force Research Laboratory, WPAFB, Ohio 45433

(Received 24 October 2005; accepted 7 March 2006; published online 16 June 2006)

Thin films of lanthanum monosulfide (LaS) have been deposited on Si (100) substrates by pulsed laser deposition. The films are golden yellow in appearance with a mirrorlike surface morphology and a sheet resistance around 0.1 $\Omega/\square$, as measured using a four-probe measurement technique. The thin films are characterized by atomic force microscopy (AFM), x-ray diffraction (XRD) analysis, high resolution transmission electron microscopy (HRTEM), ellipsometry, and Raman spectroscopy. The root-mean-square variation of (1 μm thick) film surface roughness measured over a 1 μm^2 area by AFM was found to be 1.74 nm. XRD analysis of fairly thick films (micrometer size) reveals the growth of the cubic rocksalt structure with a lattice constant of 5.863(7) Å, which is close to the bulk LaS value. HRTEM images reveal that the films are comprised of nanocrystals separated by regions of amorphous material. Two beam bright field TEM images show that there is a strain contrast in the Si substrate right under the interface with the LaS film and penetrating into the Si substrate. This suggests that there is an initial epitaxial-like growth of the LaS film on the Si substrate that introduces a strain as a result of the 8% lattice mismatch between the film and substrate. Ellipsometry measurements of the LaS films are well characterized by a Drude-Lorentz model from which an electron concentration of about 2.52×10^{22} cm^{-3} and a mobility around 8.5 cm^2/V s are derived. Typical crystalline LaS features were evident in Raman spectra of the films, but the spectra also revealed their disordered (polycrystalline) nature. © *2006 American Institute of Physics*. [DOI: 10.1063/1.2201998]

I. INTRODUCTION

Rare-earth monosulfides, in their rock salt structure, offer a more stable alternative to alkali metals in reaching low or negative electron affinity (LEA/NEA) when deposited on, for example, various III-V semiconductor surfaces.[1] Of particular interest is the room temperature work function (WF) of these chalcogenides. When extrapolated from high-temperature measurements,[2] these are found to be quite low (around 1 eV). One therefore expects that these materials can be used to reach the NEA condition when deposited onto *p*-type semiconductors. One advantage of rare-earth sulfides is that many of them are closely lattice matched to most commonly studied III-V compounds. For instance, bulk lanthanum monosulfide (LaS) has a lattice constant (5.857 Å) very close to the lattice constant of indium phosphide (InP, 5.8688 Å). Neodymium sulfide (NdS) has a lattice constant of 5.69 Å, very close to the lattice constant of gallium arsenide (GaAs, 5.6533 Å). Two other important features of the rocksalt form of these rare-earth monosulfides are their relatively high melting temperature (>2000 °C) and their fairly low electrical resistivity (a few tens of $\mu\Omega$ cm).[3]

In 2001, Modukuru *et al.* reported the growth of bulk samples of LaS and NdS using the sesquisulfide route.[4] A carbon reduction process during the high-temperature annealing portion of the growth process was shown to greatly reduce the presence of oxysulfide impurity phases (La_2O_2S and Nd_2O_2S) in the samples.[4] A picture of a LaS pellet prepared in a high-temperature induction furnace from Thermal Technologies, Inc., is shown in Fig. 1. Several of these pellets were prepared using the carbon reduction technique until enough material was produced to form a 2 in. diameter 1/8 in. thick target which was then sintered in the high-temperature furnace. The resulting target was then used for pulsed laser deposition (PLD) of LaS thin films. A preliminary account of the growth of LaS films in their cubic rocksalt structure on (100) Si substrates was reported recently.[5] In this paper, we give details of our investigation of the LaS thin films electrical and optical properties.

II. EXPERIMENT

In the PLD experimental set up,[6] the target to substrate distance was set equal to 5 cm and the high-vacuum chamber base pressure was about 8×10^{-8} Torr. All the films were grown on polished (100) silicon substrates, which were prepared using a standard cleaning procedure. A Lambda Physik LPX 305 excimer laser operating at a wavelength of 248 nm was used for the deposition. The beam spot size on the target was about 1×3 mm^2, and the laser power was set to

[a]Electronic mail: marc.cahay@uc.edu

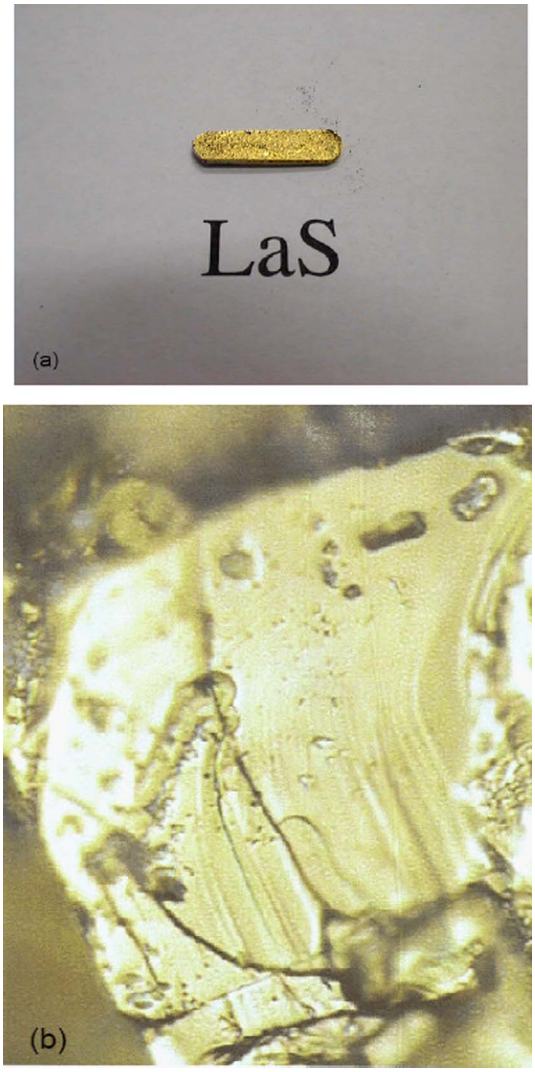

FIG. 1. (a) Picture of a LaS pellet about 1 in. long, 0.5 cm wide, and 5 mm thick formed prior to fabricating the LaS target for PLD deposition. (b) Optical micrograph of one LaS pellet showing a microcrystal of LaS about 30 μm^2 in area.

800 mJ/pulse. Approximately 56% of the laser energy is attenuated by the time the pulse reached the target due to losses from beam steering optics and the chamber window. Thus the amount of energy per pulse reaching the target is approximately 355 mJ/pulse. During deposition, the target was rotated on axis, while galvanometers were used to raster the laser beam in a uniformly random pattern over the surface of the target. This configuration produces a uniform laser plume by preventing uneven erosion of the target. A homogeneous laser plume is critical for producing films with uniform thickness. Using a laser repetition rate of 40 Hz, with a substrate temperature of 100 °C and no background gas pressure, the film growth was estimated to be about 20 nm/min for the set of PLD parameters listed above. The thin films were characterized using x-ray diffraction (XRD) at a grazing angle from 1° to 3° using a RIGAKU D-2000 model XRD machine. To investigate the texture of the films, cross-section transmission electron microscopy (TEM) samples were prepared following standard procedures. Two bars were cut out of a wafer, and were glued together with

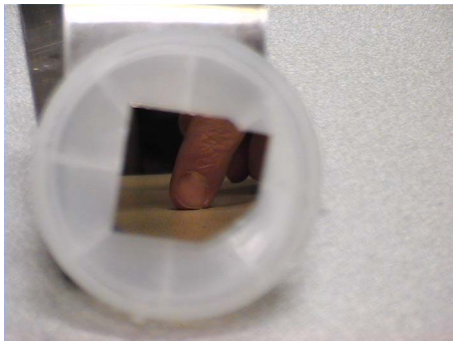

FIG. 2. Picture of a LaS thin film grown by PLD on a (100) Si substrate. The reflection of the finger clearly shows the metallic character of the thin film.

the LaS film sides face to face to make the central part of the 3 mm diameter cross-section sample disk. The disk was then mechanically thinned to ~100 μm thickness. The thinned disk was dimpled from both sides with 3 μm diamond paste until the center of the disk was ~20 μm thick, and then polished from both sides with 1 μm diamond paste to get a very smooth surface. The final thinning to produce sample perforation was conducted using Ar ion milling from both sides with an ion beam angle of 9° and a gun voltage of 6 kV. The TEM sample was examined in a Philips EM430T microscope operating at 250 kV. Variable-angle spectroscopic ellipsometry (VASE, J. A. Woollam Co., Lincoln NE) measurements were performed on the sample, from 275 to 1700 nm (4.5–0.73 eV), at six different angles of incidence ranging from 60° to 85°. The complex permittivity of the LaS film was extracted from the ellipsometric data, assuming that the film was homogeneous and no scattering.

The Raman scattering experiments were carried out in an ambient atmosphere of helium gas at a temperature of 295 K in a quasibackscattering Brewster-angle geometry[7] with the incident light at an angle of 77.7° from the normal to the LaS film surface. Spectra were excited with 150 mW of 457.9 nm argon laser light. The incident laser light formed a slit shaped spot of dimensions 1×0.1 mm^2 on the sample, which together with the use of the stream of He gas flowing over the sample in the laser spot area helped minimize the local laser heating. The light scattered at 90° (external to the sample) was analyzed with a Spex 14018 double monochromator at a spectral resolution of 7.8 cm^{-1}, and detected with a cooled RCA 31034A photomultiplier. The incident light was polarized in the scattering plane, while the scattered light was recorded without polarization analysis. Spectrometer calibrations were made immediately before and after each sample spectrum was recorded.

III. EXPERIMENTAL RESULTS

As shown in Fig. 2, the LaS films are golden yellow in appearance with a mirrorlike surface morphology. The sheet resistance of the thin films was measured to be about 0.1 $\Omega/\square$ using a four-probe measurement result. As shown on a typical plot in Fig. 3, atomic force microscopy (AFM) scans of the LaS film (about 1 μm thick as determined by TEM analysis) over a 1 μm^2 area reveal a root-mean-square

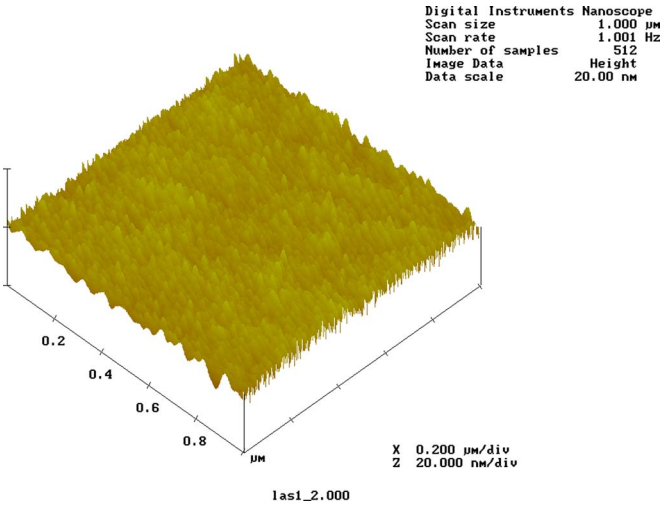

FIG. 3. AFM scan of a LaS thin film (about one micron thick) grown on a (100) Si substrate. The scan is over 1 μm^2. The root mean square of the surface roughness is 1.743 nm over that area.

(rms) variation in the surface roughness of 1.743 nm. This high smoothness of the film was verified over the entire area of the sample shown in Fig. 2.

A. XRD results

Figure 4 shows a typical XRD scan of the golden-yellow LaS thin film. The XRD scan reveals principal Bragg reflections of the cubic rocksalt phase. An analysis of the Bragg reflection peaks leads to a lattice parameter of $a=5.863(7)$ Å, which is very close (0.1% larger) than the value we reported earlier for bulk samples, $a=5.857(2)$ Å.[2–4] The observation of many Bragg reflection peaks suggests that the film is polycrystalline, which is to be expected because of the large lattice mismatch (about 8%) between the lattice constant of the LaS rocksalt phase and of the Si substrate ($a=5.431$ Å). Furthermore, the Bragg peaks are fairly broad suggesting the presence of polycrystalline grains of different sizes and potentially the presence of amorphous regions in the film. Using Scherrer's equation,[8,9] the size of the

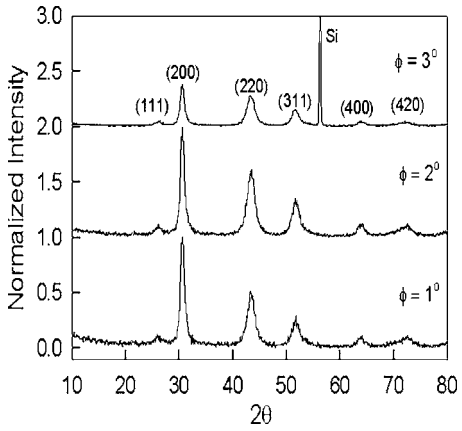

FIG. 4. X-ray diffraction at three different grazing angles of incidence (ϕ) from a LaS thin film deposited on a (100) Si substrate. Miller indices (hkl) of the reflections from the cubic rocksalt phase of LaS are identified. The peak located around 56° is due to the (311) Bragg reflection observed for a bare Si substrate (JCPSD Card No. 77-211).

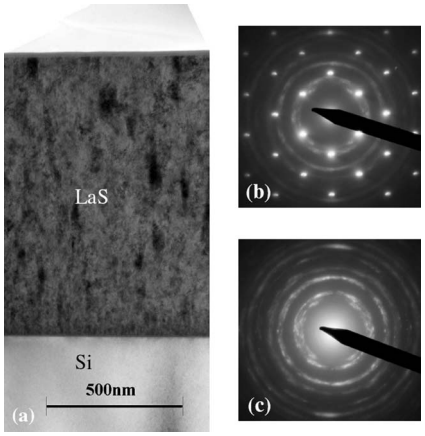

FIG. 5. (a) ⟨011⟩ zone axis bright field cross-section TEM image of the LaS films on the (100) Si substrate. (b) Corresponding electron diffraction pattern from both the LaS film and Si substrate. (c) Electron diffraction pattern from the LaS film only.

nanocrystalline grains in the film can be estimated from the full width at half maximum of the Bragg peaks while taking into account a linewidth correction for x-ray instrumentation broadening. Starting with the (200) Bragg peak in Fig. 4 and using $\lambda=1.541$ Å for the wavelength of the Cu $K\alpha$ line, the average size of the nanocrystalline grains in the LaS film is found to be about 12.7 nm. This estimate agrees well with cross-section TEM analysis of the LaS thin film, as described next.

B. TEM results

Figure 5 shows a ⟨011⟩ zone axis bright field cross-section TEM image [Fig. 5(a)] of the LaS films on the (100) Si substrate, the corresponding electron diffraction pattern from both the LaS film and Si substrate [Fig. 5(b)], and the electron diffraction pattern from the LaS film only [Fig. 5(c)]. The thickness of the film is measured from the image as 0.98 μm. In addition to the diffraction spots from the Si single crystal diffraction pattern of ⟨011⟩ zone axis, there are discontinuous rings as well in Fig. 5(b) that are from the LaS film, as shown in Fig. 5(c). The diffraction pattern of Fig. 5(c) means that the LaS film consists of nano/microcrystal and amorphous phases. This finding was confirmed by HR-TEM observations. Figures 6 and 7 are HRTEM lattice im-

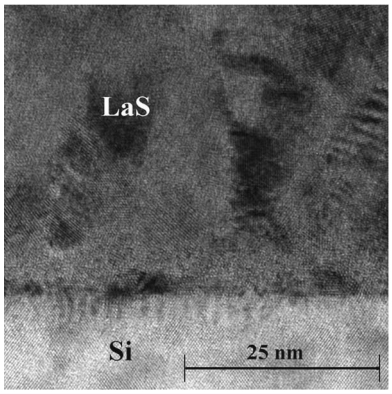

FIG. 6. HRTEM image of the LaS/Si interface clearly showing the nanocrystalline and amorphous regions.

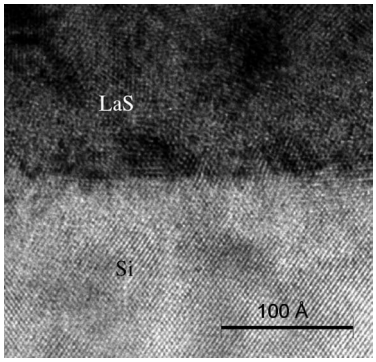

FIG. 7. Same as Fig. 6 at higher resolution.

ages of the LaS film on the Si substrate. These images reveal the existence of randomly oriented nanocrystals and amorphous regions in the proportion of approximately 60%–40%, respectively. A close inspection of the lattice image of the interface region in Fig. 7 shows an initial epitaxial growth of the LaS on the Si substrate. Figure 8 is a ⟨011⟩ bright field cross-section TEM image taken with $g=400$. In this image, the band of dark contrast in the Si substrate is a measure of the residual strain evident in the LaS film. The strain in the LaS films could arise from the thermal mismatch during the cooling from the growth temperature to room temperature due to the different thermal expansion coefficients of the LaS film and Si substrate and/or from the initial epitaxial growth of the LaS film on Si substrate due to the different lattice parameters of LaS and Si. The lattice mismatch strain is 8% assuming that the lattice parameters are 5.863 and 5.431 Å for LaS and Si, respectively.

C. Ellipsometric characterization

The measured ellipsometric data ψ and Δ of the LaS thin film are shown in Figs. 9(a) and 9(b), respectively. These spectra were modeled using Drude-Lorentz types of oscillators:

$$\varepsilon = \varepsilon_\infty - \frac{A_D \Gamma_D}{E^2 + i\Gamma_D E} + \sum_n \frac{A_n \Gamma_n E_n}{E_n^2 - E^2 - i\Gamma_n E} = \varepsilon_1 + i\varepsilon_2. \quad (1)$$

The resulting permittivity dispersion curve fits very well the experimental data using two Lorentzians in the expansion

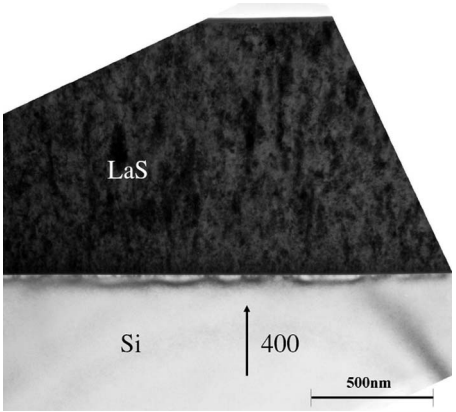

FIG. 8. $g=400$ bright field TEM image showing the strain contrast between the LaS and Si substrate interface.

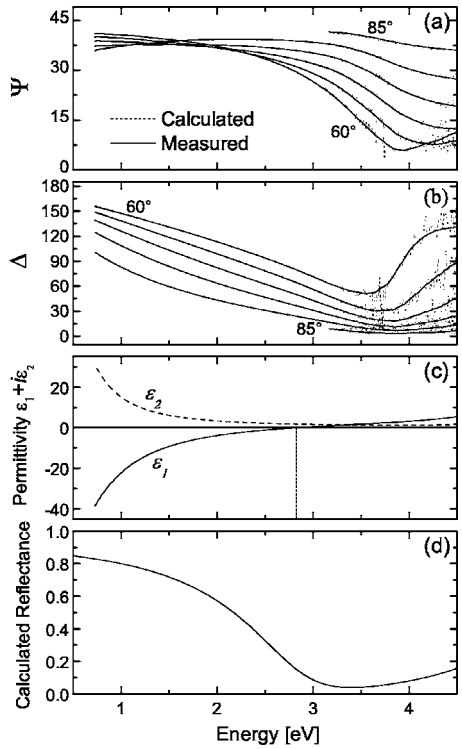

FIG. 9. Ellipsometry parameters (a) $\psi(E)$ and (b) $\Delta(E)$ of a LaS thin film grown by PLD on a (100) Si substrate. The continuous lines represent the fits to the experimental values (dashed lines) using a Drude-Lorentz model. (c) Extracted permittivity dispersion curves ε_1 and ε_2 of the LaS thin film. (d) Expected reflectance spectrum of the LaS thin film calculated from the Drude-Lorentz model.

above with the values of the parameters listed in Table I, as shown in Fig. 9(c). The parameters A_D and Γ_D in the Drude term were used to extract the carrier concentration and the mobility of LaS, 2.52×10^{22} cm^{-3} and 8.5 cm^2/V s, respectively, assuming an effective mass $m^*=1.3m_0$.[10] The carrier concentration is comparable with values given for bulk LaS.[10] In order to increase slightly the quality of the experimental fit, a 3.5 nm thick oxide layer was added to the model. From the permittivity values we deduced a minimum absorption coefficient $\alpha\approx138$ cm^{-1} and a maximum penetration depth $1/\alpha\approx70$ nm, which was not large enough to probe information related to the LaS/Si interface. From the estimates of the electron concentration and mobility reported above and a measured film thickness of 0.98 μm, the sheet resistance of the thin film is calculated to be 0.29 $\Omega/\square$, which is in good agreement with the four-probe measurement result.

For comparison with prior reports on LaS, a reflectance spectrum was calculated from the Drude-Lorentz model, as shown in Fig. 9(d). Its shape is typical of monochalco-

TABLE I. Parameters used in Eq. (1) to fit the ellipsometric data (with $\varepsilon_\infty=2.5469$).

Oscillator	A (eV)	Γ_n (eV)	E_n (eV)
Drude	3.5514	7.5164	⋯
Lorentz 1	825.19	0.455 77	0.037 278
Lorentz 2	5.1043	0.287 54	5.1043

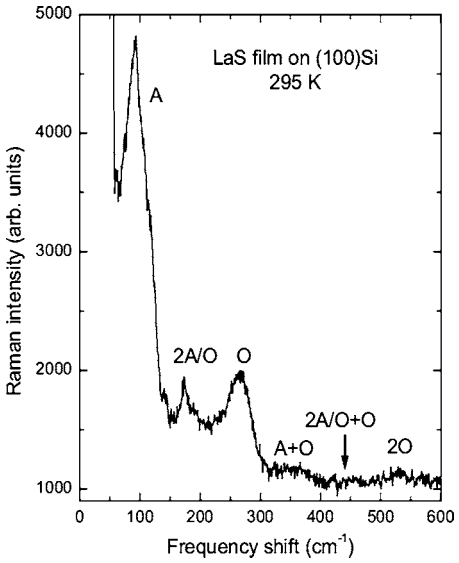

FIG. 10. Room temperature Raman spectrum of a LaS film grown on (100) Si. *A* and *O* refer to acoustic and optical phonons involved in first-order and second-order Raman scatterings.

genides, and similar to published reflectance measurements,[10,11] with (i) a metallic behavior below 2 eV due to the $5p$ quasi-free-electrons, (ii) a drop of the reflectance around 3 eV due to a conduction-electron plasma oscillation interfering with interband excitations ($f \rightarrow d, p \rightarrow d$), and (iii) an increase of the reflectance at higher energies, mainly caused by $3p \rightarrow 5d$ interband transitions.[11] An energy of 2.8 eV for the conduction-electron plasma resonance in the presence of interband transition is found, given by $\varepsilon_1 = 0$.[11] This energy is slightly larger than the previously reported value of 2.6 eV for bulk LaS,[10] may be due to the polycrystalline nature of the films.

D. Raman characterization

The Raman spectra of these Si:LaS films exhibit weak broad features extending out to 600 cm^{-1}, as illustrated in Fig. 10. The results obtained are generally similar, but not in detail, to those found earlier from Raman measurements on bulk pure LaS samples,[4,12] confirming that the LaS films are pure and mostly crystalline. Strong peaks are observed at 91 and 264 cm^{-1}, with weaker features at 120, 141, 174, 183, 365, 420, 455, and 532 cm^{-1}.

One triply degenerate optical phonon mode, split into longitudinal (LO) and transverse (TO) components, is expected for rare-earth monochalcogenides possessing the rocksalt crystal structure. First-order Raman scattering from phonons in such crystals is symmetry forbidden and usually a weak second-order Raman spectra is observed reflecting the two-phonon density of states (DOS). However, previous Raman studies of other rare-earth chalcogenides[13,14] have shown that disorder introduced by defects such as cation and/or anion vacancies[14] can induce a first-order Raman spectrum reflecting the one-phonon DOS. The TEM analysis of our samples shows that structural disorder due to the formation of nanocrystals separated by amorphous material is also present. Thus the Raman spectrum of our LaS films can be expected to show both disorder-induced first-order as well as second-order Raman features. In fact, our results for LaS resemble quite closely those obtained for GdS by Güntherodt *et al.*[13]

The strong features at 91 and 264 cm^{-1} are clearly due to disorder induced first-order Raman scattering from acoustic (A) and optic (O) phonons.[12–14] Inelastic neutron scattering measurements of the acoustic phonon dispersion in LaS (Ref. 15) allow us to determine the origins of the acoustic Raman features. The 91 cm^{-1} peak arises primarily from transverse acoustic (TA) and longitudinal acoustic (LA) phonons at the X and K critical points in the Brillouin zone, while the shoulder at 120 cm^{-1} comes mainly from L point TA and LA phonons. Unfortunately, the dispersion curves for LaS optical phonons are not known, but by analogy with those found for yttrium monosulfide (YS) (Ref. 16) only a small overall TO-LO splitting can be expected for LaS. Thus the main peak at 264 cm^{-1} comprises contributions from both TO and LO phonons, with the highest frequency contributions from LO modes. The contributions from TO modes can extend to lower frequencies, and the broad feature near 183 cm^{-1} underlying the sharper feature at 174 cm^{-1} could represent such contributions. A similar assignment has been made for other rare-earth chalcogenides from Raman spectroscopy[12–14] and also from point contact spectroscopy,[14] but the assignment is not definite.[12,13] This is because this so-called TO peak[12] overlaps with second-order Raman scattering from acoustic modes. Such scattering is generally found to be quite strong in bulk rare-earth chalcogenides.[4,12–14] However, this is not the case in our thin films. From the neutron scattering results,[15] the sharp peak at 174 cm^{-1} can be associated with second-order Raman scattering from TA and LA phonons at the X point, where there is a sharp and strong peak in the one-phonon DOS. The underlying broad peak at 183 cm^{-1} referred to above could arise from second-order scattering from TA and LA phonons at the K point. The weak peak at 141 cm^{-1} is of unknown origin.

The broad and very weak bands occurring at frequencies higher than the optic phonon peak are all second order in origin reflecting primarily combinations of the disorder-induced first-order DOS Raman peaks. For example, the peaks at 365, 455, and 532 cm^{-1} can be attributed to the combinations of the 91 and 120 (A) cm^{-1} peaks with the 264 (O) cm^{-1} peak ($A+O$), $2A/O+O$ (see Fig. 10), and $O+O$, respectively.

IV. CONCLUSIONS

Thin films of lanthanum monosulfide (LaS) have been deposited on Si (100) substrates by pulsed laser deposition (PLD). The films are golden yellow in appearance with a mirrorlike surface morphology and a sheet resistance below 1 $\Omega/\square$. The root-mean-square variation of (1 μm thick) film surface roughness measured over a 1 μm^2 area by AFM was found to be below 2 nm. XRD analysis reveals the successful growth of the cubic rocksalt structure with a lattice constant of 5.863(7) Å, which is close to the bulk LaS value. High resolution TEM (HRTEM) images indicate that the films are comprised of nanocrystals separated by regions of amorphous material. Ellipsometry measurements of the LaS

films are well characterized by a Drude-Lorentz model from which an electron concentration of about 2.52×10^{22} cm^{-3} and a mobility around 8.5 $cm^2/V\,s$ are derived. Both crystalline and disordered LaS features were evident in Raman spectra of the films.

These rare-earth sulfide thin films should have potential applications in vacuum microelectronics if they can be used to reach NEA/LEA at the surface of various III-V and II-VI compound semiconductors. Applications would include microwave vacuum transistors and tubes, pressure sensors, thin panel displays, and high-temperature and radiation tolerant sensors.

[1]P. D. Mumford and M. Cahay, J. Appl. Phys. **79**, 2176 (1996).
[2]The room temperature work function for LaS and NdS was calculated by extrapolating measured work function values at high temperature [S. Fomenko, *Handbook of Thermionic Properties* (Plenum, New York, 1966)]. Within the range of temperature investigated by Fomenko, the work function increases with temperature at a rate of a few meV/K.
[3]G. V. Samsonov, *High Temperature Compounds of Rare-Earth Metals with Nonmetals* (Consultants Bureau Enterprises, Inc., New York, 1965).
[4]Y. Modukuru, J. Thachery, H. Tang, A. Malhotra, M. Cahay, and P. Boolchand, J. Vac. Sci. Technol. B **19**, 1958 (2001).
[5]S. Fairchild, J. Jones, M. Cahay, K. Garre, P. Draviam, P. Boolchand, X. Wu, and D. J. Lockwood, J. Vac. Sci. Technol. B **23**, 318 (2005).
[6]D. B. Chrisley and G. K. Hubler, *Pulsed Laser Deposition of Thin Films* (Wiley Interscience, New York, 1999).
[7]D. J. Lockwood, M. W. C. Dharma-Wardana, J.-M. Baribeau, and D. C. Houghton, Phys. Rev. B **38**, 2243 (1987).
[8]C. J. Doss and R. Zallen, Phys. Rev. B **48**, 15626 (1993).
[9]R. Jenkins and R. L. Snyder, *Introduction to X-ray Powder Diffractometry* (Wiley Interscience, New York, 1996), p. 90.
[10]W. Beckenbaugh, J. Evers, G. Büntherodt, E. Kaldis, and P. Wachter, J. Phys. Chem. Solids **36**, 239 (1975).
[11]V. N. Antonov, B. N. Harmon, and A. N. Yaresko, Phys. Rev. B **69**, 094404 (2004).
[12]I. Frankowski and P. Watcher, Solid State Commun. **40**, 885 (1981).
[13]G. Güntherodt, P. Grünberg, E. Anastassakis, M. Cardona, H. Hackfort, and W. Zinn, Phys. Rev. B **16**, 3504 (1977).
[14]A. Treindl and P. Wachter, Phys. Lett. **64A**, 147 (1977).
[15]M. M. Steiner, H. Eschrig, and R. Monnier, Phys. Rev. B **45**, 7183 (1992).
[16]P. Roedhammer, W. Reichardt, and F. Holtzberg, Phys. Rev. Lett. **40**, 465 (1978).